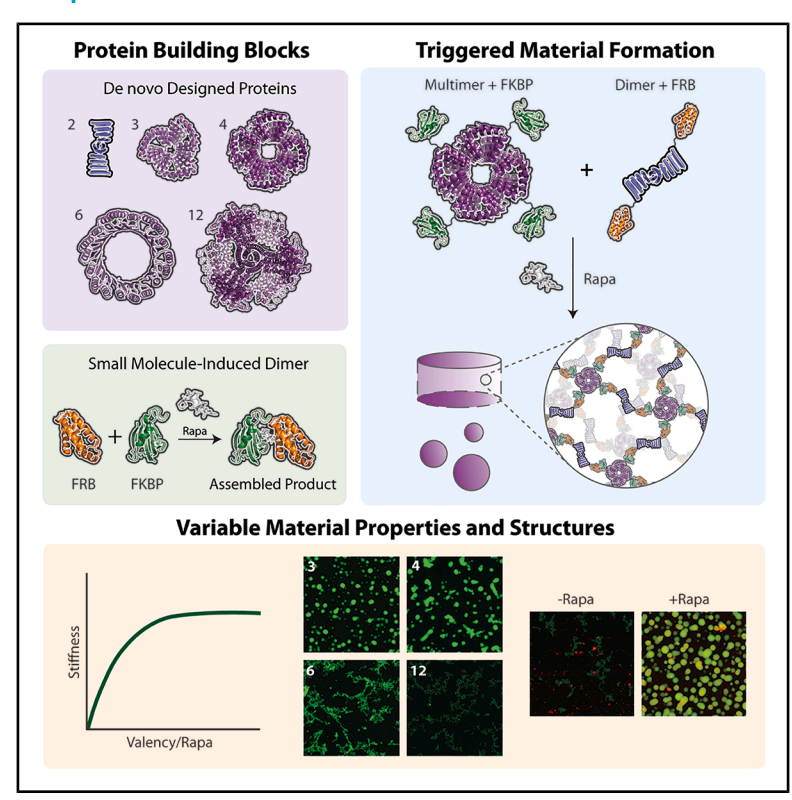
Stimuli-triggered formation of *de novo*-designed protein biomaterials

Graphical abstract



Highlights

- Self-assembling multimeric proteins are created using de novo design methodologies
- Gel and condensates form via small molecule-mediated protein heteropolymerization
- Material viscoelasticity readily tuned with protein structure and rapamycin addition

Authors

Nicole E. Gregorio, Zhe Li, Jack W. Hoye, David Baker, Cole A. DeForest

Correspondence

profcole@uw.edu

In brief

This work introduces a modular platform for creating protein-based biomaterials using *de novo-*designed proteins that self-assemble into hydrogels and condensates upon small-molecule addition. By tuning protein valency and trigger concentration, the material's mechanical properties and formation dynamics are precisely controlled. These materials can be formed both *in vitro* and *in cellulo*, offering new tools for studying biomolecular condensates and enabling the development of customizable, responsive biomaterials for biomedical and synthetic biology applications.



Please cite this article in press as: Gregorio et al., Stimuli-triggered formation of de novo-designed protein biomaterials, Cell Biomaterials (2025), https://doi.org/10.1016/j.celbio.2025.100239

Cell Biomaterials



Article

Stimuli-triggered formation of *de novo*-designed protein biomaterials

Nicole E. Gregorio, ¹ Zhe Li, ^{2,3,4} Jack W. Hoye, ^{5,6} David Baker, ^{3,4} and Cole A. DeForest ^{1,4,5,6,7,8,9,*}

¹Department of Bioengineering, University of Washington, Seattle, WA 98105, USA

https://doi.org/10.1016/j.celbio.2025.100239

THE BIGGER PICTURE Biomaterials are revolutionizing how we study biology and treat diseases, offering new platforms for tissue engineering, drug delivery, and cellular modulation. Among these, protein-based materials stand out for their ability to mimic biological environments with unmatched precision. Despite this, most protein hydrogels rely on a narrow set of naturally occurring building blocks, limiting their versatility. This work introduces a new frontier in biomaterials by leveraging *de novo* protein design, a computational approach that creates entirely new proteins from scratch. By engineering proteins that self-assemble into defined architectures and respond to external stimuli, such as small molecules, we demonstrate the creation of customizable bulk hydrogels and intracellular condensates with tunable mechanical properties and formation dynamics.

These materials not only expand the toolkit for bioengineers but also provide a powerful platform for probing fundamental biological processes. For example, the ability to trigger condensate formation inside cells opens new avenues for studying intracellular liquid-liquid phase separation, a phenomenon increasingly linked to aging and disease. Moreover, the modularity of this system, where protein components and triggers can be swapped, suggests broad applicability across biotechnology, synthetic biology, and regenerative medicine. As *de novo* design continues to evolve, it promises to unlock a vast landscape of protein-based materials with properties and functions beyond what nature has provided, reshaping how we build and interact with biological systems.

SUMMARY

Protein-based biomaterials have risen in popularity in recent years owing to their genetic encodability, sequence specificity, monodispersity, and ability to interface with biological systems in comparison with synthetic polymer-based materials. Though naturally derived and minimally engineered proteins have been at the forefront of these efforts, recent advances in computational protein design offer exciting opportunities for next-generation biomaterial development. In this work, we employ *de novo* protein design methodologies to generate a suite of self-assembling multimeric proteins, whose step-growth heteropolymerization into bulk hydrogels and condensates can be exogenously triggered through small-molecule addition. Our results highlight how changes in programmed multimer valency and their triggered assembly yield materials with varying structures and viscoelasticity. We anticipate that these approaches will prove useful in rapidly generating large libraries of stimuli-responsive biomaterials that are precisely tailored to specific applications in the biosciences and beyond.

²Department of Biomedical Engineering, Southern University of Science and Technology, Shenzhen 518055, China

³Department of Biochemistry, University of Washington, Seattle, WA 98105, USA

⁴Institute for Protein Design, University of Washington, Seattle, WA 98105, USA

⁵Department of Chemical Engineering, University of Washington, Seattle, WA 98105, USA

⁶Institute of Stem Cell & Regenerative Medicine, University of Washington, Seattle, WA 98105, USA

⁷Department of Chemistry, University of Washington, Seattle, WA 98105, USA

⁸Molecular Engineering & Sciences Institute, University of Washington, Seattle, WA 98105, USA

⁹Lead contact

^{*}Correspondence: profcole@uw.edu



INTRODUCTION

Biomaterials have provided us with a multitude of new approaches to study biological systems and devise novel medical treatments. Hydrogels have been of particular interest for potential use as three-dimensional (3D) cell culture matrices, tissue engineering scaffolds, and therapeutic delivery vehicles. 1,2 Historically, hydrogels have most typically been constructed from synthetic polymers. More recently, protein-based hydrogels have gained additional popularity in the biomedical space due to their improved ability to replicate biological microenvironments both chemically and structurally.3-6 Many such materials rely on naturally occurring proteins extracted from biological samples or those which have been recombinantly expressed, potentially with minor redesigns to better suit their intended application. This work has led to an impressive collection of protein-based biomaterials with varied mechanical and responsive properties.^{3,7} Of specific note in the responsive materials space, hydrogels with triggerable formation have proven to be essential for many applications. These materials enable more straightforward cell encapsulation, in vivo formation, and secondary network polymerization within an existing material.^{8,9}

Despite the many unique and desirable properties of recombinant proteins-namely their perfect sequence specificity and monodispersity, intrinsic biofunctionality and biodegradability, and scalable synthesis through fermentation - most biomaterials based on these structures have been constructed from a surprisingly limited number of building blocks used as intrinsically disordered linkers (e.g., elastin-like polypeptides, XTEN), crosslinking chemistries (e.g., Tag/Catcher chemistries, coiled-coil interactions), and responsive domains (e.g., PhoCl, Dronpa, and calmodulin).6,10-14 While these efforts have proven useful in many applications, recent advances in computational protein design near-limitlessly expand the available space for biomaterials development. De novo design has already enabled the creation of countless new-to-nature proteins with demonstrated utility as multivalent vaccines and protein binders. 15 Especially with the advent of diffusion-based methods like RoseTTAFold diffusion (RFdiffusion), 16 de novo design is well poised to transform the future of protein engineering, with its impacts undoubtedly extending into the realm of protein-based materials.

In the first report of its kind, our labs recently demonstrated the potential in using *de novo*-designed proteins for hydrogel synthesis. ¹⁷ Using self-assembling multivalent protein oligomers fused to crosslinking protein domains, macroscopic materials with varied viscoelastic properties were formed spontaneously upon component mixing. This work demonstrated that modifications of the individual protein components, including linker lengths, geometries, and valencies, can give rise to significant changes in bulk material properties. However, the rapid and spontaneous formation of these materials can limit their application, especially in biological contexts where controlled formation is often more replicative of natural processes. As such, the integration of controlled formation in *de novo* materials would be a great step forward in enabling simultaneous user control over both material properties and material formation.

This previous work also provided evidence that these *de novo* materials could be formed within cells due to their genetically en-

coded nature. Such intracellular materials are reminiscent of biomolecular condensates, or localized, membraneless compartments within the cell cytoplasm. Condensates play diverse and essential roles in maintaining cellular organization and facilitating a variety of cellular processes. 18 As such, when condensate regulation goes awry cells can enter a diseased state, and this has been identified as a driver of various age-related diseases like neurodegeneration, cancer, and cardiovascular disease. 18-21 Carefully controlled material properties are paramount to a condensates' ability to perform its intended functions. 18,22-24 Condensates are typically dynamic in nature and form through multivalent physical interactions between biomolecules but can vary from more liquid-like to more gel or solid-like states.²⁵ However, solid-like condensates are often disease related, as the less dynamic state may halt processes that are necessary to maintain cell health.^{23,26} In other biological systems, liquid-like protein condensates can even serve as precursors for formation of solid materials, such as silk fibers and mussel threads.²⁷⁻²⁹ We have only just begun to understand the intricacies of condensates. New engineered condensate systems, especially those with triggerable formation or state changes, are key in better studying the complex interplay of condensate structure, state, and function.^{30–3}

In this work, we sought to create a suite of *de novo*-designed proteins whose step-growth heteropolymerization into bulk networks could be exogenously controlled through small-molecule addition. To do so, we utilized a set of *de novo* proteins designed to assemble into distinct nanostructures of different valencies and fused them to a small-molecule-responsive protein pair. Here, we demonstrate that the resulting two-component systems can be used to form macroscopic hydrogel materials with different viscoelastic behaviors. We also show that material properties can be further controlled by modifying the amount of small-molecule trigger added to the system. Additionally, inspired by previous evidence of similar materials forming intracellular structures resembling biomolecular condensates, ^{17,30,31} we further characterized the behavior of the system at low protein concentrations to investigate its ability to form such structures in a controlled fashion.

RESULTS

Protein design

This platform utilizes *de novo* protein design to build a library of material-forming proteins (Figure 1A). We started by identifying previously *de novo*-designed proteins that self-assemble with known valencies. In contrast to previous work, we focused on low valencies that are more heavily utilized in synthetic polymer-based materials. We identified existing designed homo-oligomers with 2, 3, 4, and 12 assembling groups. Additionally, we used RFdiffusion to design a homo-hexamer to complete the set (Figure 1B). Negative-stain electron microscopy (nsEM) was used to confirm the assembly valency and overall shape of the selected hexamer design (Figure S1).

To template network-level assembly of these proteins, we sought to create a two-component system where each multimer (3, 4, 6, and 12) would be paired with the same dimer core. Assembly of the multimer/dimer pairs would be driven by heterodimeric proteins pairs with user-controlled association. We selected the naturally occurring FK506 binding protein



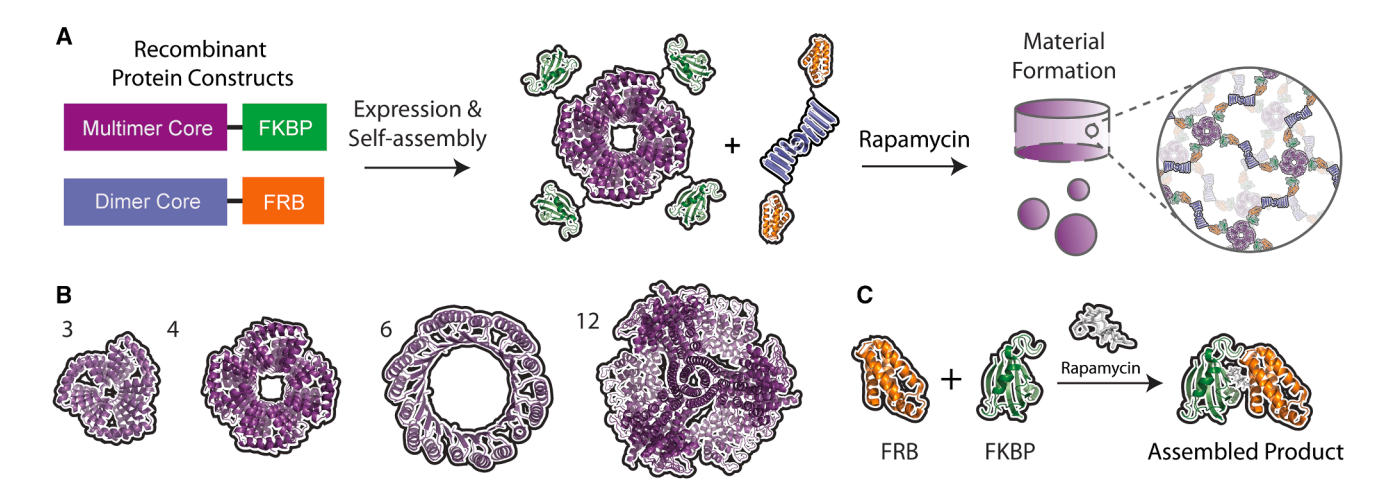


Figure 1. Library design of triggerable condensate-forming proteins

(A) This system utilizes self-assembling core proteins expressed as genetic fusions through a flexible linker to one component of a crosslinking protein pair. Upon expression, these polypeptides self-assemble into multimers of the noted valency. Following small-molecule addition, multimer and dimer species heteropolymerize into bulk hydrogels or microscopic condensed phases.

(B) Multimer cores of various valencies used in this system.

(C) FKBP/FRB proteins used as crosslinks for this system. These proteins natively associate only in the presence of the small-molecule rapamycin. Protein data base: FKBP/FRB—3FAP.

(FKBP)/FKBP-rapamycin binding domain (FRB) protein pair, whose noncovalent association is controlled by the presence of the small-molecule rapamycin⁴¹ (Figure 1C). We genetically fused the FRB protein to the dimer-forming polypeptide and the FKBP protein to the multimer component, including a short flexible $5\times$ Gly-Gly-Ser linker between each. This results in structures whose assembly valency is the same as its number of crosslinking proteins and allows for a network of interactions to be initiated between the two components. For nomenclature, we refer to each network forming multimer/dimer pair by the valency of the multimer (e.g., 3 or 3mer for materials formed from the dimer-FRB + trimer-FKBP proteins). All polyhistidine-tagged proteins were individually recombinantly expressed in E. coli, purified by immobilized metal affinity chromatography, and concentrated as needed for the formation of 10 wt % bulk materials. The identity of each protein was confirmed by sodium dodecyl sulfate-polyacrylamide gel electrophoresis (SDS-PAGE) and mass spectrometry (Figure S2).

Impact of valency on bulk hydrogel properties

We first sought to characterize the bulk materials formed by all combinations of these proteins. When each multimer/dimer pair is combined with equal FRB:FKBP stoichiometry and 10 wt % total protein concentration, the mixture persists as a liquid as expected. However, when rapamycin is added to the mixture at an equimolar concentration, a hydrogel-like material forms, facilitated by FKBP/FRB association. Each valency was characterized by rheology to determine sample storage modulus and viscoelastic properties (Figure 2A). We hypothesized that materials formed from higher valency multimers would result in stiffer constructs given the increased potential interconnectedness of these networks.

Rheology revealed that increased multimer valency generally results in increased material stiffness, up to a certain point. A trend

of increasing stiffness is seen between the 3, 4, and 6mers, at which point the stiffness levels off, with the 6mer and 12mer displaying very similar stiffnesses. We hypothesize that at a certain valency threshold, steric hinderance due to the highly colocalized crosslinking points may prevent many crosslinks from forming, leading to greater defects in the network and offsetting the expected increase in stiffness. We were encouraged to see these trends despite the additional complexities of the structures we are comparing. It is challenging to untangle the contributions of various properties other than valency that may also affect the material stiffness, such as differences in protein molecular weights, relative rigidity of the multimer structures, and possible variation in the position (axial vs. equatorial) of crosslinking domains relative to the multimer core (Figure S3). Despite these complexities, this library of proteins covers many intermediate stiffness in the 0-1 kPa range, which is typical for protein-based materials and overlaps with that of many soft tissue environments. 42

In addition to stiffness, we also characterized the frequency-dependent behavior of these materials (Figures 2B and 2C). As the rapamycin-mediated association of FKBP/FRB is noncovalent, these physically crosslinked materials exhibit a frequency crossover point—at low frequencies, the loss modulus (G") dominates and the material exhibits a viscous state; at high frequencies, the storage modulus (G') dominates and the material exhibits an elastic state. This crossover occurs regardless of the multimer used, with the crossover frequency decreasing consistently with increased construct valency. The trend in decreasing frequency crossover holds between the 6mer and 12mer despite their similar stiffnesses, though it is not statistically significant.

Controlled hydrogel stiffness using rapamycin

The ability to select multimer valency provides an initial level of versatility to this system. However, since multimer/dimer



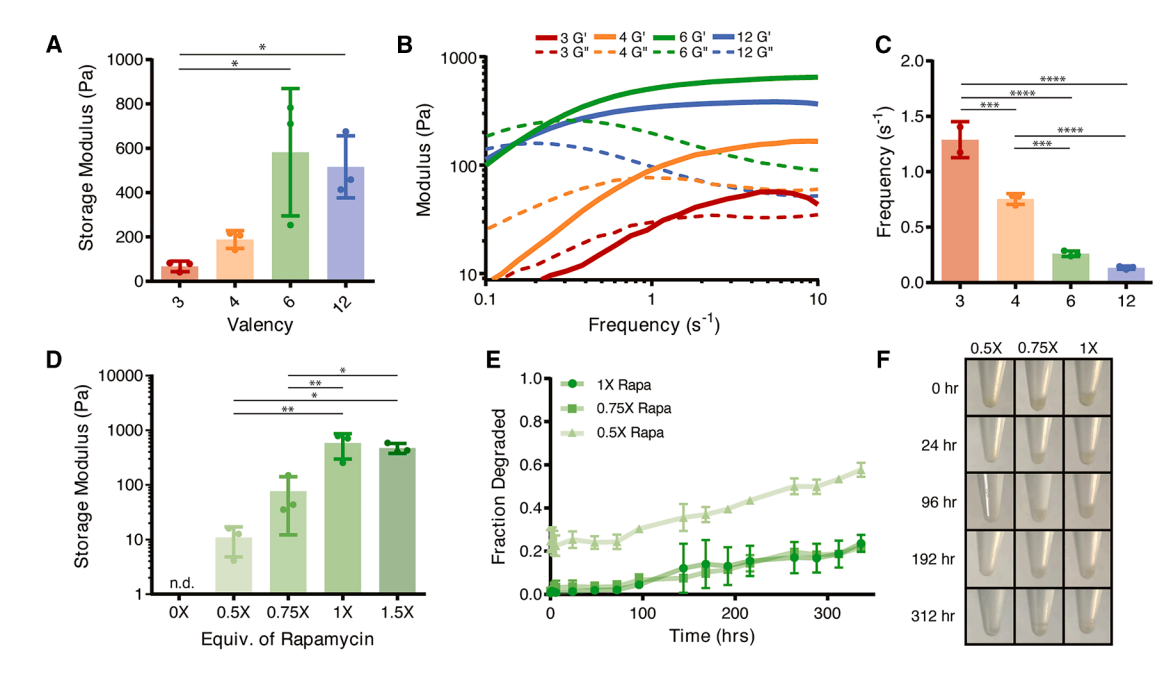


Figure 2. Characterization of the viscoelasticity and stability of bulk materials

(A) G' determined from oscillatory rheology time sweeps at 25°C, 1% shear strain, and 5 s⁻¹ angular frequency with 10 wt % FKBP/FRB crosslinked gels at an equimolar concentration of rapamycin to FRB/FKBP. Bars represent the mean ± SD of three independently formed gels. Significance testing was performed using Tukey's multiple comparisons test.

- (B) A representative frequency sweep test at 25°C with fixed 1% shear strain for 10 wt % FKBP/FRB crosslinked gels at an equimolar concentration of rapamycin to FRB/FKBP.
- (C) Frequency crossover points determined from frequency sweep data. Bars represent the mean ± SD of three independently formed gels. Significance testing was performed using Tukev's multiple comparisons test.
- (D) G' determined from oscillatory rheology time sweeps at 25° C, 1% shear strain, and 5 s⁻¹ angular frequency with 6mer 10 wt % FKBP/FRB crosslinked gels at varying ratios of rapamycin to FRB/FKBP. Bars represent the mean \pm SD of three independently formed gels. Significance testing was performed using Tukey's multiple comparisons test.
- (E) Extent of gel degradation over 14 days under ambient conditions with varied rapamycin. Each point represents the mean ± SD of three independently formed gels.
- (F) Images of representative gels at time points throughout the degradation study.

association is mediated through small-molecule addition, we hypothesized that overall material state and viscoelasticity could be dynamically altered using varying amounts of rapamycin. To characterize the responsive behavior of the system, additional rheological studies were performed on the 6mer system held at a fixed protein concentration while varying rapamycin relative to FRB/FKBP (Figure 2D). Adding sub-stoichiometric rapamycin concentrations resulted in significantly softer materials, as expected; under these conditions, an insufficient amount of rapamycin is present to saturate all available FKBP/FRB pairs, resulting in a less-crosslinked network with increased defects. At excess rapamycin no additional gains in stiffness are seen, and there is potential to saturate FKBP/FRB sites, preventing proper interaction. As such, rapamycin both initiates material formation and modulates the final stiffness of the material that is formed.

Despite increased defects at sub-stochiometric rapamycin concentrations, gel erosion studies show that gels formed with rapamycin equivalents of $0.75\times$ or greater are highly stable over 14 days. Only $\sim\!20\%$ of the material eroded at this point and minimal differences in the degradation profile are observed as compared with $1\times$ rapamycin (Figures 2E and 2F). At $0.5\times$ rapamycin, erosion is more rapid; up to 60% of the material is

eroded by day 14 and an immediate burst release of >20% of protein is observed, likely as a result of a high fraction of completely unbound protein.

Impact of valency on condensate formation

Next, we aimed to utilize the same set of proteins to create microscopic condensate-like structures. To do so, we first performed phase diagram analysis of each pair in the presence of equimolar rapamycin to determine the conditions necessary for condensate formation (Figures 3A and 3B). We screened a variety of protein concentrations (0-5 μM) alongside differing amounts of a molecular crowding agent-poly(ethylene glycol) (PEG, 0-5 wt %). All valencies led to formation of microscale structures, with the conditions for formation and morphology varying for each. For the 3mer and 4mer, 2 wt % PEG was required for clear condensation to occur. Higher valencies were capable of forming condensed structures at 1 or even 0 wt % PEG. While changes in the protein concentration did not make the difference between condensation or no condensation, the number and morphology of condensates did vary. Most notably, the 3mer and 4mer showed more rounded, droplet-like morphologies at high protein and PEG concentrations, as



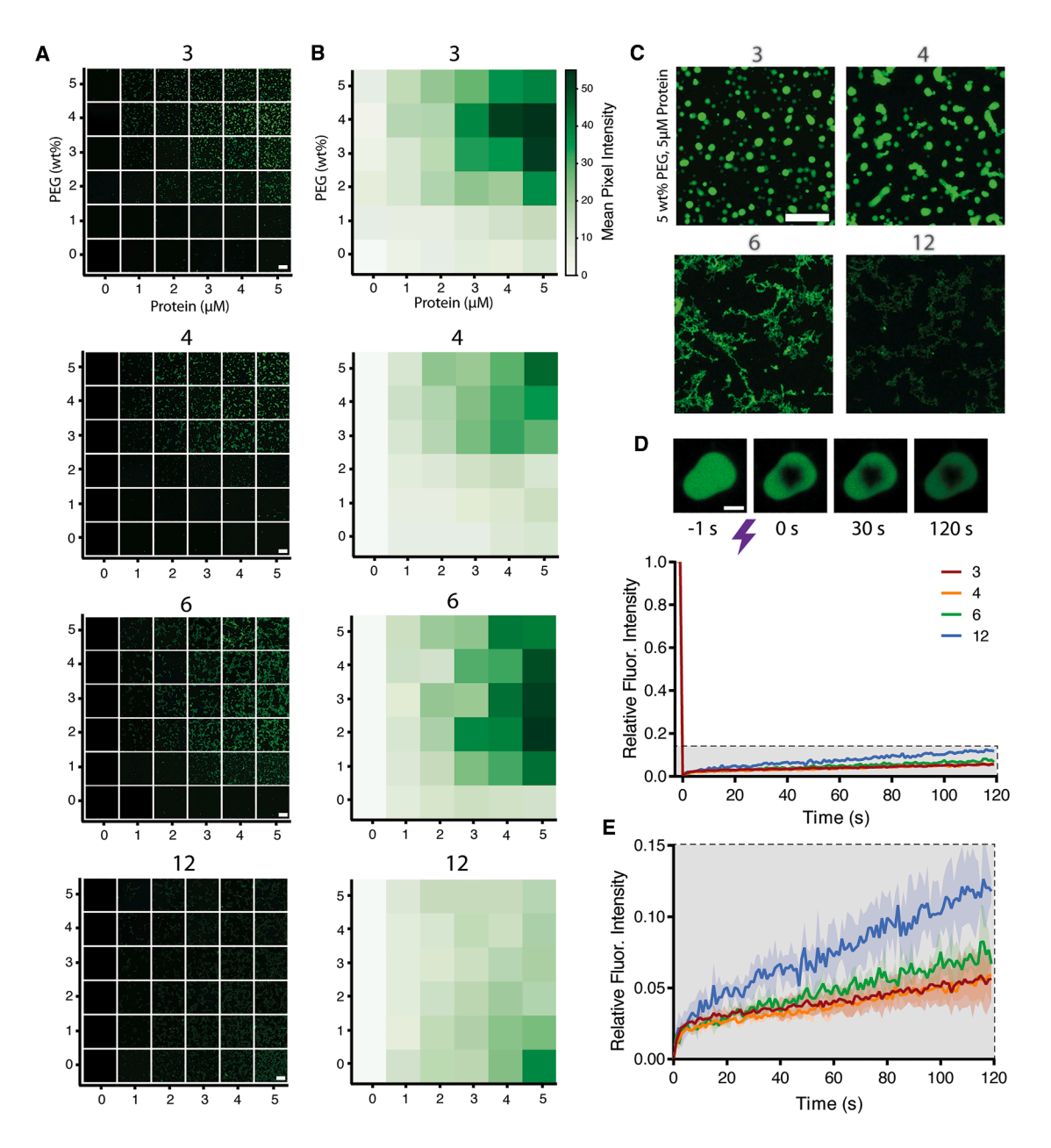


Figure 3. Characterization of phase separation behavior

(A) Phase diagrams of each valency. Dimer protein is fluorescently tagged with FAM for tracking. Images represent maximum projections of z stacks over 10 μm. Scale bars, 20 μm.

- (B) Mean fluorescence intensity of phase diagram images quantified in Fiji.
- (C) Comparison of condensed phase morphology across valencies at 5 wt % PEG and 5 µM total protein. Scale bars, 20 µm.
- (D) FRAP in condensed phases formed at 5 wt % and 5 μM total protein. Bleaching was carried out for 200 ms with a 405-nm laser, and samples were monitored at 1 s intervals for 120 s after bleaching. Each line represents the mean of three separate bleaching events, and the shaded area represents the SD. Scale bars, 2 μm. (E) Zoom in of shaded area of graph from (D).

opposed to more aggregated structures at lower concentrations. Similar changes in condensed phase morphology occurred with differences in valency, where under the same conditions lower valencies formed droplet-like structures and higher valencies formed aggregated structures (Figure 3C). We also performed phase diagram analysis on the dimer protein alone, identifying low levels of aggregate-like structures (Figure S4). However, all

dimer-only conditions gave fewer and less bright condensed phases than any of the multimer/dimer pairs. This may indicate that there is some background aggregation of the dimer protein that is mostly overcome in the presence of a multimer.

We hypothesized that these morphological differences may be reflective of differences in the material properties of these condensed phases. Other work in the condensates space has



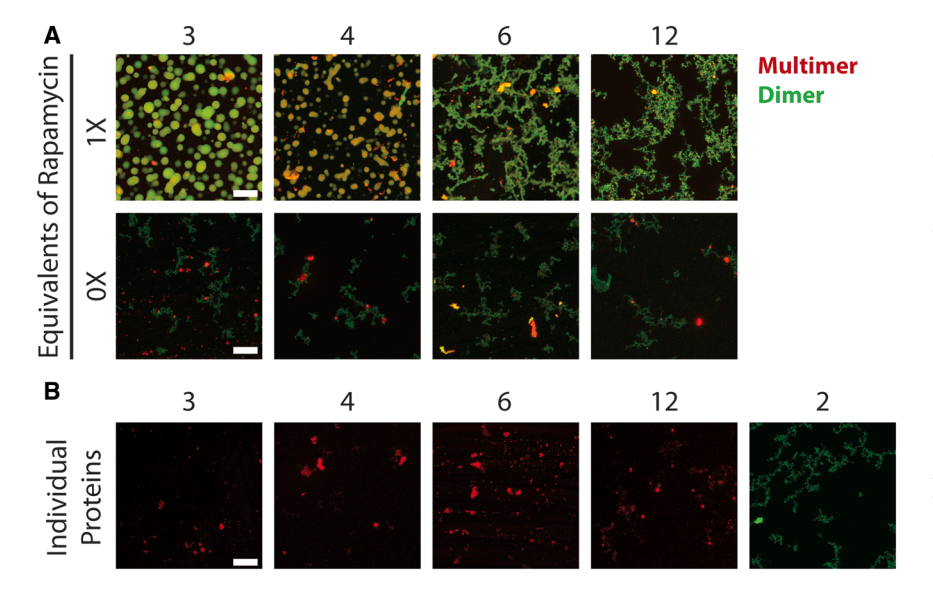


Figure 4. Dependence of condensate formation on rapamycin

(A) Comparison of each multimer/dimer pair with and without rapamycin. Multimer proteins are NHS labeled with Cy5 and the dimer with FAM for tracking. All mixtures are prepared at 5 wt % PEG and 5 μ M total protein.

(B) Individual proteins prepared as in (A) for identification of background aggregation. All images represent maximum projections of z stacks over 10 μ m. Scale bars, 10 μ m.

Controlled condensate formation using rapamycin

As with the bulk materials, we wanted to demonstrate the ability to trigger formation of this condensed phase with small-molecule addition. We see a clear difference in the condensed phases when rapamycin is included or excluded

(Figures 4A and S7). With rapamycin, all valencies show colocalization of the multimer, labeled with Cyanine5 (Cy5), and dimer indicating their interaction, whereas without rapamycin colocalization is mostly lost and the morphology of the condensed phase changes. In comparison with the multimer and dimer proteins individually (Figure 4B), we observed that multimer/dimer protein mixtures without rapamycin resemble the morphology of their respective individual proteins, further indicating that rapamycin is necessary for interactions between proteins to occur. It is notable that there is some level of apparent condensed phase formation resulting from aggregation of these proteins with themselves.

We also tracked condensate formation after rapamycin addition in real time to further demonstrate the triggerability of this system (Figure 5A; Videos S6, S7, S8, and S9). Condensates appear to form rapidly after the addition of rapamycin but take additional time to settle to the bottom of the sample for imaging. Comparison of condensate morphology at 60 min versus overnight (as in Figure 3C) reemphasizes the long timescale at which these structure fuse and rearrange.

Finally, we aimed to identify changes in condensed phase structures with varied amounts of rapamycin. Similarly to bulk materials, we anticipated that lower amounts of rapamycin would result in more liquid-like condensates. However, condensate morphology for the 3mer was only minorly affected by such changes (Figures 5B and S8). We noticed the appearance of some smaller condensates with decreased rapamycin, particularly in the 0.1× condition. Similar characterization of the other valencies also resulted in few noticeable differences in the overall morphology across rapamycin concentrations (Figure S9). We also performed FRAP analysis on 3mer condensates with varied amounts of rapamycin, finding that all conditions displayed similar minimal recovery (Figure 5C; Videos S10, S11, S12, and \$13). These results indicate that either changes in material properties in response to varied rapamycin are outside of the range of detection of these methods, or that these changes simply do not translate to the microscopic scale. For example, it may be

demonstrated that spherical morphologies often indicate more liquid-like material states, whereas irregular morphologies are indicative of more gel or solid-like states. 31,43 To test this, we performed fluorescence recovery after photobleaching (FRAP) analysis on each of these valencies under the same conditions (Figure 3D; Videos S1, S2, S3, and S4). While FRAP does not provide a direct readout of the stiffness of these materials, it provides a measurement of the diffusivity of the dye-labeled molecule, which often correlates with the physical state of the material when a condensate scaffold protein is labeled. 44-46 We opted to tag the dimer-FRB protein with fluorescein (FAM) for tracking, as this protein is used with all valencies and should provide us with a direct look at the rearrangement of the structures. Multimer-FKBP proteins were left unlabeled. For all valencies. <15% fluorescence recovery was detected over the span of 2 min, indicating minimal rearrangement within these condensates. While increased valency appears to result in slight gains in the fluorescence recovery, which would indicate higher diffusivity, it is likely that these small differences are a result of the morphological differences between samples rather than representative of actual differences in material properties. Extended FRAP over 10 min as well as single-particle tracking data on the 3mer corroborated that minimal rearrangement is seen on this timescale (Figure S5; Video S5). This was unexpected due to the noncovalent nature of the crosslinks, and the ability of bulk materials to show frequency-dependent changes in behavior. However, it is worth noting that the rapamycin-FRB-FKBP complex is known to be exceptionally stable, with a dissociation constant of ~12 nM.41 As such, rearrangement of these protein complexes may occur on a much longer timescale than is detectable by these methods. For example, centrifugation of 3mer condensates immediately after rapamycin addition allowed for these structures to be more easily tracked as they developed (Figure S6). Over the first 20 h of formation, significant changes in the morphology of the condensed phase are seen alongside nearby condensate fusion, indicating some level of rearrangement over these longer timescales.



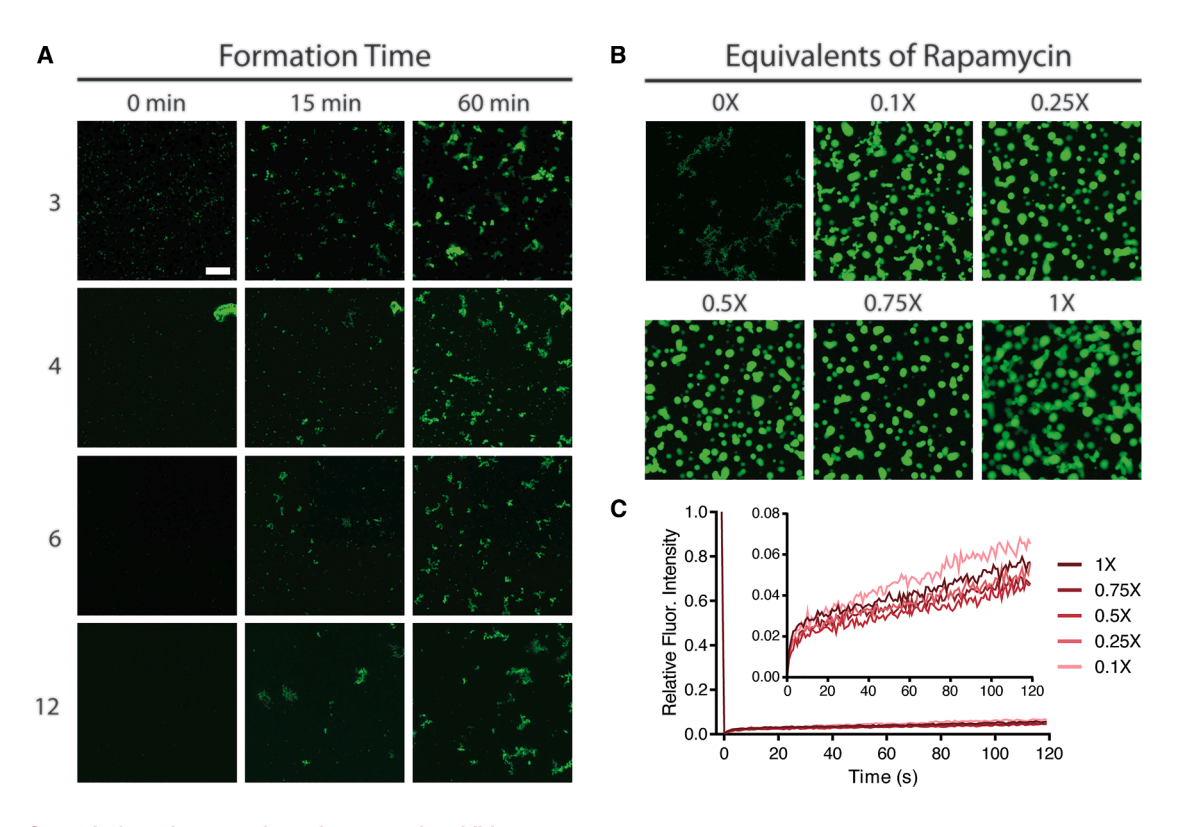


Figure 5. Control of condensates through rapamycin addition

(A) Triggered formation of a condensed phase via addition of rapamycin to the protein mixture. Rapamycin is added at 0 min.

(B) Comparison of condensed phase morphology for the 3mer at varying ratios of rapamycin. All images represent maximum projections of z stacks over 10 μm. Scale bars. 10 μm.

(C) FRAP in 3mer condensed phases with varying ratios of rapamycin. Bleaching was carried out for 200 ms with a 405-nm laser, and samples were monitored at 1 s intervals for 120 s after bleaching. Each line represents the mean of three separate bleaching events. All mixtures are prepared at 5 wt % PEG and 5 µM protein and the dimer protein is NHS labeled with FAM for tracking.

possible that rapamycin accumulates in the condensed phase over time, resulting in similar extents of crosslinking across variable concentrations, and that protein in excess of the amount of rapamycin stays in the dilute solution phase.

Finally, we aimed to replicate rapamycin-triggered formation of condensates within cells (i.e., *in cellulo*). To do so, we created HEK293T cells with doxycycline-inducible stable expression of a green fluorescent protein (GFP)-tagged dimer and transient expression of an mCherry-tagged 6mer via transfection. Treating these cells with rapamycin resulted in the appearance of bright puncta with colocalized red and green fluorescence, similar to what we observed when combining purified versions of these proteins (Figure S10). In contrast, cells expressing both proteins but not treated with rapamycin show evenly distributed fluorescence throughout the cell body, with no clear condensation as expected. This promising result highlights the unique advantage of working with entirely protein-based systems for their ease of translation into biological systems.

DISCUSSION

In this work, we demonstrated the utility of *de novo*-designed proteins as novel building blocks for triggered protein-based material formation at the macro- and microscopic scales. Our

strategy utilizes self-assembling *de novo* proteins designed to form multimeric and dimeric cores fused to crosslinking protein pairs, enabling multimer/dimer binding upon bridging small-molecule addition. This simple approach is modular, where the multimer, dimer, and crosslinking pair can all be swapped out to result in new materials with unique physical and responsive properties. Here, we demonstrate that by selecting multimers of different valencies, each equipped with small-molecule responsiveness, we can control the physical properties of bulk hydrogels and modify condensate morphology. *De novo* protein design provides a unique opportunity to rapidly iterate and redesign systems such as these to suit a given application, something that is difficult to achieve using rational design approaches.

Notably, this work builds on previous efforts in this space ¹⁷ by newly implementing a responsive crosslinking protein pair, FKBP/FRB. In doing so, we demonstrate that these materials can be programmed to respond to user-controlled stimuli; specifically, this approach permits controlled initiation of material formation and extent of crosslinking through the variable addition of the small-molecule rapamycin. New protein-based hydrogels, such as these, may have utility as 3D cell culture or delivery platforms. Especially, given the ability to control material gelation, encapsulation of cells would be straightforward. However, rapamycin is known to bind to native FKBP in mammalian cells,



activating FKBP's allosteric inhibition of mammalian target of rapamycin (mTOR), a key kinase in a master regulator pathway that controls cell growth and metabolism. Since the mTOR pathway is dysregulated in many diseases, including cancer and neurological diseases, rapamycin has been used as a drug to treat such diseases, often in combination with other therapies. As such, it may be useful to identify alternative chemically inducible dimerizers if this system is to be implemented in a biological context. While FKBP/FRB is by far the most well-studied chemically induced dimerizer, alternatives such as Pyl/ABI and GID1/GAI, both of which are derived from plants, may be useful for increasing bioorthogonality. As,49 Furthermore, de novo design has shown potential for designing novel chemically inducible dimers based on pre-selected small molecules.

Finally, we show that these de novo protein nanostructures can be triggered to form condensate-like structures at low concentrations and inside cells. Due to the use of rapamycin-inducible crosslinking, these condensate structures form only in response to the addition of this small molecule, as was seen with bulk materials. Additionally, previous studies have shown that increasing multivalency in condensate-forming biomolecules increases their propensity for phase separation. 36,51-53 Thus, we expected that higher valencies would result in condensate formation at lower molecular crowding conditions than lower valencies, which was demonstrated in our phase diagram analysis. While we aimed to show that changes to multimer valency and rapamycin concentration resulted in modification of condensate materials properties, we found that we were unable to recapitulate the trends seen in bulk materials. While changes in valency and rapamycin concentration had some impact on condensate morphology, all condensates showed little propensity for protein rearrangement. This could be a result of the exceptional low dissociation constant of the FKBP/FRB/rapamycin complex, deficiencies in the techniques utilized for such characterization, or could represent a differential impact of multivalency and network defects at the microscopic scale.

The ability of these proteins to form condensate-like structures may prove useful for further investigation into the role and impact of condensates in cells. Protein-based systems can be easily implemented in cells, and, as we have demonstrated, external application of rapamycin can induce intracellular condensation. While the use of rapamycin may obfuscate any conclusion about the direct impact of these condensates, we see this work as a steppingstone to such applications. Utilization of de novo proteins for intracellular condensate formation may prove particularly useful in achieving a level of biorthogonality that is not possible when utilizing known condensate-forming proteins in the mammalian proteome. 31,54 Thus, we may be better able to isolate the effects of condensate material properties for example, as these de novo proteins are less likely to impact other essential biological pathways within the cell. Future work to develop de novo proteins that have more varied physical properties, including those that display more liquid-like states, might provide a useful comparison.

While beyond the scope of this initial report, we anticipate that the protein pair used for crosslinking of these materials could easily be replaced with other stimuli-responsive protein pairs to modify the responsive behavior. For example, the recently introduced light-activated SpyLigation (LASL) could be used to more spatiotemporally control formation of these protein-based biomaterials as well as their final viscoelasticity. 55,56 Emerging protein engineering techniques, including *de novo* design, could even be used to create new responsive protein pairs, which may similarly prove useful for the aforementioned applications. 57

Ultimately, we believe that this work provides evidence that *de novo* design has the potential to change the way that protein-based materials are created and exponentially expand the diversity of such materials. Most notably, we have demonstrated that *de novo* materials can be created with triggerable behaviors, like small-molecule-induced material formation. While we believe our modular system of design is a useful starting point, there are surely a multitude of alternative design approaches achievable through *de novo* design that could result in materials with variable responsive behaviors. *De novo* design has the potential to create protein-based materials with properties we have not seen or imagined before.

METHODS

6mer design and validation

Denoising diffusion model RFdiffusion was used to design novel protein oligomers with 6-fold (C6) symmetry. From 100 diffusion runs generating C6-symmetric structures with 100 amino acids per chain, 22 scaffold designs were selected based on visual inspection for desirable secondary structure, oligomeric interactions, and overall geometry. Unstructured termini were trimmed to improve design quality. For each of the 22 selected protein oligomer scaffolds, ProteinMPNN model was used to generate 20 sequence designs. These sequences were then predicted for their folding and oligomer assembly using Superfold (github.com/rdkibler/superfold), a convenience wrapper for AlphaFold2,⁵⁸ with an initial structure guess protocol.⁵⁹ Designs were filtered using a predicted local distance difference test (pLDDT) threshold of 90 and a tolerance of 0.2, resulting in 20 high-confidence candidates. These were visually inspected, and 3 top designs were chosen for experimental validation.

Each of the top designs was expressed and purified as described in the following section. Protein expression and purity were assessed by SDS-PAGE. Soluble designs with correct molecular weights were further purified by size-exclusion chromatography (SEC) on a Superose 6 Increase 10/300 column (Cytiva) using running buffer (25 mM Tris, 150 mM NaCl, and pH 8.0). SEC-purified proteins were concentrated using 10 kDa molecular weight cutoff centrifugal filters (Amicon) and quantified by NanoDrop (A280) prior to downstream assembly and characterization. Out of the three, two designs expressed solubly and showed monodisperse peaks by SEC.

Oligomeric assembly was confirmed by nsEM. 6 μ L of protein sample was applied on negatively glow-discharged, formvar/carbon-supported 400-mesh copper grids (Ted Pella) for more than 2 min. The grid was blotted and stained with 3 μ L of 0.75% uranyl formate, blotted again, and stained with another 3 μ L of uranyl formate for 20 s before final blotting. Imaging was performed on a 120 kV Talos L120C transmission electron microscope (TEM; Thermo Scientific). For image data processing, nsEM datasets were processed by CryoSPARC software.



Micrographs were imported into the CryoSPARC web server, and the contrast transfer function was corrected. Around 100 particles were manually picked and classified in two dimensions. Selected classes were used as templates for particle picking in all images. All the picked particles were two-dimensionally classified for 20 iterations into 50 classes. Particles from selected classes were used for building the *ab initio* initial model. The initial model was homogeneously refined using C6 symmetry. The design with the higher soluble expression yield was selected for further hydrogel development.

Protein expression and purification

Cloned plasmids were designed in house and purchased from GenScript. All plasmids are available through Addgene (Dimer-FRB: 239847, 3mer-FKBP: 239848, 4mer-FKBP: 239849, 6mer-FKBP: 239851, and 12mer-FKBP: 239852), and amino acid sequences can be found in the supplemental text. These plasmids were transformed into electrocompenent BL21(DE3) *E. coli* for protein expression.

BL21(DE3) *E. coli* containing the plasmid of interest were grown overnight in Lysogeny broth (LB). Fresh Terrific broth (TB) medium was combined with kanamycin and inoculated at 1:10 with overnight culture. The culture was grown at 37°C and 200 rpm for 4–5 h until the optical density (OD)600 was 0.7–1.0, at which point 0.5 mM isopropyl β -D-1-thiogalactopyranoside (IPTG) was added, and the culture was moved to 18°C, 200 rpm overnight. Cells were harvested by centrifugation at 4,000 \times g for 20 min at 4°C. Cell pellets were frozen at -80°C prior to purification.

Cell pellets, each derived from ~500 mL of culture, were resuspended in 40 mL of lysis buffer (300 mM NaCl, 25 mM Tris, 5 mM imidazole, and pH 8) supplemented with 1 mM phenylmethylsulfonyl fluoride (PMSF). Resuspended cells were placed in an ice-water bath and sonicated at 80% amplitude for 2 min of total on time in 1-s on, 1-s off intervals (Fisherbrand, Model 505 Sonic Dismembranator, 0.5-in probe). Cell lysate was centrifuged at $10,000 \times g$ for 45 min at 4°C, and the supernatant was collected for purification. Ni-NTA HisTag affinity chromatography was conducted using an ÄKTA Pure 25 L with a HisTrap column (Cytiva). Cell lysate was loaded onto the column, then it was thoroughly washed (300 mM NaCl, 25 mM Tris, 40 mM imidazole, pH 8) and the protein eluted (300 mM NaCl, 25 mM Tris, 500 mM imidazole, and pH 8.0). Collected elution fractions containing protein were buffer exchanged into Tris-buffered saline (TBS, 50 mM Tris, 200 mM NaCl, and pH 7.4) using a 10 kDa molecular weight cutoff spin concentrator and finally concentrated to ~100 mg mL⁻¹ by NanoDrop (A280). Concentrated stocks were flash frozen in liquid nitrogen and stored at -80°C until use.

Hydrogel formation

All hydrogels were formed at 10 wt % total protein and with 1:1 matched FKBP:FRB stoichiometry. Rapamycin was purchased from LCLab, and stock solutions were prepared by dissolving in dimethyl sulfoxide (DMSO). The amount of rapamycin to add was determined by ensuring that the rapamycin:FKBP molar ratio was 1:1. For testing with less than 1 equiv of rapamycin, amounts were adjusted such that $0.5 \times \text{rapamycin}$ means rapa-

mycin:FKBP is 0.5:1. The total DMSO concentration in the gels was held constant at 3.3% v/v by compensating for additional volume needed after rapamycin addition with pure DMSO. Due to the low solubility of rapamycin in water, the following order of addition to form gels was followed to minimize precipitation during formation: multimer, TBS, DMSO, rapamycin, and dimer. Gelation occurs rapidly after addition of the dimer.

Rheological characterization

Rheology was performed on an Anton Paar Physica MCR 301 using an 8-mm-diameter parallel-plate geometry with a 0.5 mm gap, at $25^{\circ}C$. $30~\mu\text{L}$ of gel was pre-formed for 1 h on a coverslip in a humidified chamber. The coverslip was then taped to the Peltier plate of the rheometer, the probe was lowered until the gel filled the geometry, and the edges were covered with mineral oil to prevent evaporation. The following testing routine was performed on each gel: time sweep (5 rad s $^{-1}$, 1% strain, 10 min); frequency sweep (0.1–200 rad s $^{-1}$, 1% strain); time sweep (5 rad s $^{-1}$, 1% strain). G' values were determined by averaging the last 10 measurements in the second time sweep. Three independently formed gels were measured for each condition.

Gel erosion

 $30~\mu L$ 6mer gels were formed in triplicate at the bottom of 1.5 mL microcentrifuge tubes with varying equivalents of rapamycin. Gels were allowed to form for 1 h at room temperature, then covered with 1 mL of TBS. Gels remained under ambient conditions throughout the course of the study and were sampled by removing 150 μL of TBS from each tube and replacing it with 150 μL of fresh TBS. Photos of the gels were also taken at each time point. After 14 days, a Pierce bicinchoninic acid (BCA) assay was performed on all samples to determine the amount of protein in each. A standard curve was constructed using known concentration of the dimer/6mer mixture at a 1:1 molar ratio, as was present in the gels. Protein content was adjusted to account for sample removal and replacement with fresh TBS and used to determine the extent of degradation of the gels at each time point.

Condensate formation

Dimer and multimer proteins were fluorescently labeled for tracking during condensate imaging. To do so, dimer protein was buffer exchanged via a spin concentrator into PBS with 100 mM sodium bicarbonate until the protein concentration was \sim 1 mg mL⁻¹. The protein solution was then combined with 12× molar excess of fluorescein N-hydroxysuccinimidyl ester (FAM-NHS) 6-isomer (Broad Pharma) dissolved in DMSO. The mixture was protected from light and left rocking at room temperature for 2 h for the labeling reaction to proceed. Finally, the mixture was buffer exchanged via spin concentration to remove excess dye, and we returned the protein to TBS before flash freezing in liquid nitrogen and storing at -80°C until use. The multimer proteins were labeled following a similar protocol but using Cy5-NHS (Lumiprobe) at a 3× molar excess. For use in condensate formation, these labeled proteins were combined with unlabeled protein at no more than a 1:20 molar ratio to ensure that labeling minimally affected condensation. Prior to use, fresh protein stocks



were thawed and centrifuged at $16,000 \times g$ for 3 min to remove any aggregates. The solution was then adjusted to the necessary concentration by NanoDrop (A280).

Condensates were formed in 384-well glass bottom black plates (Cellvis) by addition of components in the following order: buffer (25 mM Tris, 100 mM NaCl, and pH 7.4), deionized water, PEG (3,350 Da), DMSO, rapamycin, multimer, and dimer. Amounts each of protein, rapamycin, and DMSO were determined as noted in the hydrogel formation section. The total concentration of protein is 5 μ M, PEG is 5 wt %, and DMSO is 6% v/v unless otherwise noted. Well plates were then sealed with parafilm to prevent evaporation and protected from light while condensate formation was allowed to proceed for 20 h prior to imaging.

All imaging was completed on a Leica Stellaris 5 confocal microscope with a $40\times$ oil immersion objective. FAM-labeled dimer was visualized with an excitation wavelength of 488 nm and an emission detection range of 493–638 nm. Cy5-labeled multimers were visualized with an excitation wavelength of 633 nm and an emission detection range of 638–779 nm. Images represent a maximum projection in z through \sim 10 μ m of the sample at 0.5 μ m increments starting from the glass surface.

FRAP

FRAP was performed on a Leica Stellaris 5 confocal microscope with a $40\times$ oil immersion objective and a 405-nm laser for bleaching. FAM-labeled dimer was visualized with an excitation wavelength of 488 nm and an emission detection range of 493–638 nm. Bleaching time was 200 ms at 90% laser power and resulted in a bleached area $\sim\!\!2~\mu m$ in diameter. Images were collected at a 1 s interval for 120 time points and analyzed using Fiji to measure the fluorescence within the bleached area and in a reference spot within an unbleached condensate at each time point. This was used to correct for photobleaching due to repeated imaging. Three independent bleaching events were imaged for each condition.

Condensate formation time courses

Time courses were captured on a Leica Stellaris 5 confocal microscope with a $40\times$ oil immersion objective. FAM-labeled dimer was visualized with an excitation wavelength of 488 nm and an emission detection range of 493–638 nm. Images were collected every 3 min for a total of 75 min, with rapamycin added after 12 min. Each frame represents a maximum projection in z through ${\sim}10~\mu m$ of the sample at 0.5 ${\mu}m$ increments starting from the glass surface.

In cellulo condensate formation

Condensates were formed inside HEK293T cells stably expressing an EGFP-tagged dimer protein and transiently transfected with plasmid encoding an mCherry-tagged 6mer protein as follows. Sleeping Beauty transposon plasmids containing the EGFP-tagged dimer under a doxycycline-inducible promoter were cloned (Genscript) and transformed into NEB10 (New England Biolabs) for maintenance and expansion. After prepping, the transposon plasmid was co-transfected into HEK293T alongside SB100×, a gift from Mark Groudine (AddGene #127909), in a transposon:Sleeping Beauty ratio of 5:1. After 3 days, HEK293T were selected using puromycin (Fischer). Cells

were expanded under selection for two weeks until 10–15 million cells were present. Then protein expression was induced with doxycycline (Fischer) for 24 h prior to confirmation of fluorescence signal via confocal microscope. Upon observation of fluorescence signal, cells were dissociated using TrypLE (ThermoFisher), pelleted at $500 \times g$ for 5 min, resuspended using FACS buffer (Hanks Buffered Saline Solution, 10 mM HEPES, and 1% BSA) to a final density of 10 million cells mL $^{-1}$, and passed through a cell strainer (Corning) into a 5 mL FACS tube. FACS was performed to capture the highest expressing cells (top 10%). After sorting, cells were centrifuged and plated into warmed DMEM (ThermoFisher, 10% FBS, $1\times$ PenStrep) and allowed to expand.

After expansion, cells were plated in 35-mm glass bottom dishes (Cell Vis) coated with 100 µL of 1% gelatin at 75,000 cells per dish. After allowing cells to attach overnight, media was replaced to remove non-adherent cells. In a separate tube, plasmids encoding the mCherry-tagged 6mer were diluted into Opti-MEM and combined with P3000 (ThermoFisher) according to manufacturer protocols. Plasmid was then mixed with diluted Lipofectamine 3000 (ThermoFisher) and allowed to incubate for 30 min to allow for nanoparticle formation. After incubation, the transfection mix was applied to plated cells. Immediately following transfection, cells were induced with doxycycline to trigger expression of the dimer protein. After 24 h, expression of both proteins was confirmed via confocal microscopy. Then rapamycin prepared at 3 mM in DMSO was diluted 1:1,000 into PBS and added to the media at a 1:10 ratio for a final concentration of 300 nM. 24 h after rapamycin addition, confocal imaging on intracellular condensates was carried out.

RESOURCE AVAILABILITY

Lead contact

Further information and requests for resources and reagents should be directed to and will be fulfilled by the lead contact, Dr. Cole A. DeForest (profcole@uw.edu).

Materials availability

All plasmids for protein expression are available through Addgene—dimer-FRB: 239847, 3mer-FKBP: 239848, 4mer-FKBP: 239849, 6mer-FKBP: 239851, and 12mer-FKBP: 239852.

Data and code availability

All data reported in this paper will be shared by the lead contact upon request. Any additional information required to reanalyze the data reported in this paper is available from the lead contact upon request.

ACKNOWLEDGMENTS

This work is supported by the National Science Foundation (DGE-2140004 to N.E.G.), the National Institutes of Health (R35GM138036 to C.A.D.), and the Defense Advanced Research Projects Agency (HR00112420369 to C.A.D. and D.B.). Mass spectrometry data were collected at the Mass Spectrometry Center at the University of Washington. The authors thank Rubul Mout, Justin Decarreau, Jack Hoye, and Cyrus Hass for helpful conversations and technical training.

AUTHOR CONTRIBUTIONS

Conceptualization, N.E.G. and C.A.D.; formal analysis, N.E.G.; funding acquisition, N.E.G., D.B., and C.A.D.; investigation, N.E.G., Z.L., and J.W.H.;



methodology, N.E.G., Z.L., and J.W.H.; resources, D.B. and C.A.D.; software, N.E.G. and Z.L.; supervision, C.A.D.; validation, N.E.G.; visualization, N.E.G.; writing (original draft), N.E.G. and C.A.D.; writing (review & editing), N.E.G., Z.L., J.W.H., D.B., and C.A.D.

DECLARATION OF INTERESTS

The authors declare no competing interests.

SUPPLEMENTAL INFORMATION

Supplemental information can be found online at https://doi.org/10.1016/j.celbio.2025.100239.

Received: June 3, 2025 Revised: September 2, 2025 Accepted: September 17, 2025

REFERENCES

- Correa, S., Grosskopf, A.K., Lopez Hernandez, H., Chan, D., Yu, A.C., Stapleton, L.M., and Appel, E.A. (2021). Translational Applications of Hydrogels. Chem. Rev. 121, 11385–11457. https://doi.org/10.1021/acs.chemrev.0c01177.
- Gharios, R., Francis, R.M., and DeForest, C.A. (2023). Chemical and biological engineering strategies to make and modify next-generation hydrogel biomaterials. Matter 6, 4195–4244. https://doi.org/10.1016/j.matt. 2023 10 012
- Jonker, A.M., Löwik, D.W.P.M., and van Hest, J.C.M. (2012). Peptide- and Protein-Based Hydrogels. Chem. Mater. 24, 759–773. https://doi.org/10. 1021/cm202640w.
- Garcia, C., Patkar, S.S., Wang, B., Abouomar, R., and Kiick, K.L. (2023). Recombinant protein-based injectable materials for biomedical applications. Adv. Drug Deliv. Rev. 193, 114673. https://doi.org/10.1016/j.addr. 2022.114673.
- Li, H., Kong, N., Laver, B., and Liu, J. (2016). Hydrogels Constructed from Engineered Proteins. Small 12, 973–987. https://doi.org/10.1002/smll. 201502429.
- Bennett, J.I., Boit, M.O., Gregorio, N.E., Zhang, F., Kibler, R.D., Hoye, J. W., Prado, O., Rapp, P.B., Murry, C.E., Stevens, K.R., et al. (2024). Genetically Encoded XTEN-based Hydrogels with Tunable Viscoelasticity and Biodegradability for Injectable Cell Therapies. Adv. Sci. (Weinh) 11, e2301708. https://doi.org/10.1002/advs.202301708.
- Wang, Y., Katyal, P., and Montclare, J.K. (2019). Protein-Engineered Functional Materials. Adv. Healthc. Mater. 8, e1801374. https://doi.org/ 10.1002/adhm.201801374.
- Davoodi, E., Li, J., Ma, X., Najafabadi, A.H., Yoo, J., Lu, G., Sani, E.S., Lee, S., Montazerian, H., Kim, G., et al. (2025). Imaging-guided deep tissue in vivo sound printing. Science 388, 616–623. https://doi.org/10.1126/science.adt/1293
- Kopyeva, I., Goldner, E.C., Hoye, J.W., Yang, S., Regier, M.C., Bradford, J. C., Vera, K.R., Bretherton, R.C., Robinson, J.L., and DeForest, C.A. (2024). Stepwise Stiffening/Softening of and Cell Recovery from Reversibly Formulated Hydrogel Interpenetrating Networks. Adv. Mater. 36, e2404880. https://doi.org/10.1002/adma.202404880.
- Sun, F., Zhang, W.-B., Mahdavi, A., Arnold, F.H., and Tirrell, D.A. (2014).
 Synthesis of bioactive protein hydrogels by genetically encoded SpyTag-SpyCatcher chemistry. Proc. Natl. Acad. Sci. USA 111, 11269– 11274. https://doi.org/10.1073/pnas.1401291111.
- Gregorio, N.E., and DeForest, C.A. (2024). PhoCoil: An Injectable and Photodegradable Single-component Recombinant Protein Hydrogel for Localized Therapeutic Cell Delivery. Preprint at bioRxiv, 2024.05.07. 592971. https://doi.org/10.1101/2024.05.07.592971.

- Lyu, S., Fang, J., Duan, T., Fu, L., Liu, J., and Li, H. (2017). Optically controlled reversible protein hydrogels based on photoswitchable fluorescent protein Dronpa. Chem. Commun. (Camb) 53, 13375–13378. https:// doi.org/10.1039/C7CC06991J.
- Lee, J.S., Kang, M.J., Lee, J.H., and Lim, D.W. (2022). Injectable Hydrogels of Stimuli-Responsive Elastin and Calmodulin-Based Triblock Copolypeptides for Controlled Drug Release. Biomacromolecules 23, 2051–2063. https://doi.org/10.1021/acs.biomac.2c00053.
- Olsen, B.D., Kornfield, J.A., and Tirrell, D.A. (2010). Yielding Behavior in Injectable Hydrogels from Telechelic Proteins. Macromolecules 43, 9094–9099. https://doi.org/10.1021/ma101434a.
- Kortemme, T. (2024). De novo protein design-from new structures to programmable functions. Cell 187, 526–544. https://doi.org/10.1016/j.cell. 2023.12.028.
- Watson, J.L., Juergens, D., Bennett, N.R., Trippe, B.L., Yim, J., Eisenach, H.E., Ahern, W., Borst, A.J., Ragotte, R.J., Milles, L.F., et al. (2023). De novo design of protein structure and function with RFdiffusion. Nature 620, 1089–1100. https://doi.org/10.1038/s41586-023-06415-8.
- Mout, R., Bretherton, R.C., Decarreau, J., Lee, S., Gregorio, N., Edman, N.I., Ahlrichs, M., Hsia, Y., Sahtoe, D.D., Ueda, G., et al. (2024). De novo design of modular protein hydrogels with programmable intra- and extracellular viscoelasticity. Proc. Natl. Acad. Sci. USA *121*, e2309457121. https://doi.org/10.1073/pnas.2309457121.
- Zhang, H., Ji, X., Li, P., Liu, C., Lou, J., Wang, Z., Wen, W., Xiao, Y., Zhang, M., and Zhu, X. (2020). Liquid-liquid phase separation in biology: mechanisms, physiological functions and human diseases. Sci. China Life Sci. 63, 953–985. https://doi.org/10.1007/s11427-020-1702-x.
- Lu, X., Lu, J., Li, S., Feng, S., Wang, Y., and Cui, L. (2024). The Role of Liquid–Liquid Phase Separation in the Accumulation of Pathological Proteins: New Perspectives on the Mechanism of Neurodegenerative Diseases. Aging Dis. 16, 769–786. https://doi.org/10.14336/AD.2024.0209.
- Tong, X., Tang, R., Xu, J., Wang, W., Zhao, Y., Yu, X., and Shi, S. (2022). Liquid-liquid phase separation in tumor biology. Signal Transduct. Target. Ther. 7, 221. https://doi.org/10.1038/s41392-022-01076-x.
- Wang, J., Gan, Y., Cao, J., Dong, X., and Ouyang, W. (2022). Pathophysiology of stress granules: An emerging link to diseases. Int. J. Mol. Med. 49, 44. https://doi.org/10.3892/ijmm.2022.5099.
- Mitrea, D.M., Mittasch, M., Gomes, B.F., Klein, I.A., and Murcko, M.A. (2022). Modulating biomolecular condensates: a novel approach to drug discovery. Nat. Rev. Drug Discov. 21, 841–862. https://doi.org/10.1038/s41573-022-00505-4.
- Alberti, S., Gladfelter, A., and Mittag, T. (2019). Considerations and Challenges in Studying Liquid-Liquid Phase Separation and Biomolecular Condensates. Cell 176, 419–434. https://doi.org/10.1016/j.cell.2018.12.035.
- 24. Woodruff, J.B., Hyman, A.A., and Boke, E. (2018). Organization and Function of Non-dynamic Biomolecular Condensates. Trends Biochem. Sci. 43, 81–94. https://doi.org/10.1016/j.tibs.2017.11.005.
- Banani, S.F., Lee, H.O., Hyman, A.A., and Rosen, M.K. (2017). Biomolecular condensates: organizers of cellular biochemistry. Nat. Rev. Mol. Cell Biol. 18, 285–298. https://doi.org/10.1038/nrm.2017.7.
- Sohn, E.J., and Libich, D.S. (2024). Squishy to crusty: Biophysics reveal the molecular details of FUS droplet maturation. Structure 32, 854–855. https://doi.org/10.1016/j.str.2024.06.007.
- Harrington, M.J., Mezzenga, R., and Miserez, A. (2024). Fluid protein condensates for bio-inspired applications. Nat Rev Bioeng. 2, 260–278. https://doi.org/10.1038/s44222-023-00133-6.
- Rising, A., and Harrington, M.J. (2023). Biological Materials Processing: Time-Tested Tricks for Sustainable Fiber Fabrication. Chem. Rev. 123, 2155–2199. https://doi.org/10.1021/acs.chemrev.2c00465.
- Miserez, A., Yu, J., and Mohammadi, P. (2023). Protein-Based Biological Materials: Molecular Design and Artificial Production. Chem. Rev. 123, 2049–2111. https://doi.org/10.1021/acs.chemrev.2c00621.

Please cite this article in press as: Gregorio et al., Stimuli-triggered formation of de novo-designed protein biomaterials, Cell Biomaterials (2025), https://doi.org/10.1016/j.celbio.2025.100239



Cell Biomaterials

- Nakamura, H., Lee, A.A., Afshar, A.S., Watanabe, S., Rho, E., Razavi, S., Suarez, A., Lin, Y.-C., Tanigawa, M., Huang, B., et al. (2018). Intracellular production of hydrogels and synthetic RNA granules by multivalent molecular interactions. Nat. Mater. 17, 79–89. https://doi.org/10.1038/ nmat5006.
- Hernandez-Candia, C.N., Brady, B.R., Harrison, E., and Tucker, C.L. (2024). A platform to induce and mature biomolecular condensates using chemicals and light. Nat. Chem. Biol. 20, 452–462. https://doi.org/10.1038/s41589-023-01520-1.
- Garabedian, M.V., Wang, W., Dabdoub, J.B., Tong, M., Caldwell, R.M., Benman, W., Schuster, B.S., Deiters, A., and Good, M.C. (2021). Designer membraneless organelles sequester native factors for control of cell behavior. Nat. Chem. Biol. 17, 998–1007. https://doi.org/10. 1038/s41589-021-00840-4.
- Hernández-Candia, C.N., Pearce, S., and Tucker, C.L. (2021). A modular tool to query and inducibly disrupt biomolecular condensates. Nat. Commun. 12, 1809. https://doi.org/10.1038/s41467-021-22096-1.
- Cao, Y., Wei, X., Lin, Y., and Sun, F. (2020). Synthesis of bio-inspired viscoelastic molecular networks by metal-induced protein assembly. Mol. Syst. Des. Eng. 5, 117–124. https://doi.org/10.1039/C9ME00027E.
- Bracha, D., Walls, M.T., Wei, M.-T., Zhu, L., Kurian, M., Toettcher, J.E., and Brangwynne, C.P. (2018). Mapping local and global liquid-liquid phase behavior in living cells using light-activated multivalent seeds. Preprint at bioRxiv, 283655. https://doi.org/10.1101/283655.
- Shin, Y., Berry, J., Pannucci, N., Haataja, M.P., Toettcher, J.E., and Brangwynne, C.P. (2017). Spatiotemporal Control of Intracellular Phase Transitions Using Light-Activated optoDroplets. Cell 168, 159–171.e14. https://doi.org/10.1016/j.cell.2016.11.054.
- Taslimi, A., Vrana, J.D., Chen, D., Borinskaya, S., Mayer, B.J., Kennedy, M. J., and Tucker, C.L. (2014). An optimized optogenetic clustering tool for probing protein interaction and function. Nat. Commun. 5, 4925. https://doi.org/10.1038/ncomms5925.
- Hsia, Y., Mout, R., Sheffler, W., Edman, N.I., Vulovic, I., Park, Y.-J., Redler, R.L., Bick, M.J., Bera, A.K., Courbet, A., et al. (2021). Design of multi-scale protein complexes by hierarchical building block fusion. Nat. Commun. 12, 2294. https://doi.org/10.1038/s41467-021-22276-z.
- Ueda, G., Antanasijevic, A., Fallas, J.A., Sheffler, W., Copps, J., Ellis, D., Hutchinson, G.B., Moyer, A., Yasmeen, A., Tsybovsky, Y., et al. (2020). Tailored design of protein nanoparticle scaffolds for multivalent presentation of viral glycoprotein antigens. eLife 9, e57659. https://doi.org/10.7554/eLife.57659.
- Bethel, N.P., Borst, A.J., Parmeggiani, F., Bick, M.J., Brunette, T.J., Nguyen, H., Kang, A., Bera, A.K., Carter, L., Miranda, M.C., et al. (2023). Precisely patterned nanofibres made from extendable protein multiplexes. Nat. Chem. 15, 1664–1671. https://doi.org/10.1038/s41557-023-01314-x.
- Banaszynski, L.A., Liu, C.W., and Wandless, T.J. (2005). Characterization of the FKBP.rapamycin.FRB Ternary Complex. J. Am. Chem. Soc. 127, 4715–4721. https://doi.org/10.1021/ja043277y.
- Guimarães, C.F., Gasperini, L., Marques, A.P., and Reis, R.L. (2020). The stiffness of living tissues and its implications for tissue engineering. Nat. Rev. Mater. 5, 351–370. https://doi.org/10.1038/s41578-019-0169-1.
- Bergsma, T., Steen, A., Kamenz, J.L., Otto, T.A., Gallardo, P., and Veenhoff, L.M. (2025). Imaging-based quantitative assessment of biomolecular condensates in vitro and in cells. J. Biol. Chem. 301, 108130. https://doi.org/10.1016/j.jbc.2024.108130.
- Wang, Z., Lou, J., and Zhang, H. (2022). Essence determines phenomenon: Assaying the material properties of biological condensates. J. Biol. Chem. 298, 101782. https://doi.org/10.1016/j.jbc.2022.101782.

- Elbaum-Garfinkle, S., Kim, Y., Szczepaniak, K., Chen, C.C.-H., Eckmann, C.R., Myong, S., and Brangwynne, C.P. (2015). The disordered P granule protein LAF-1 drives phase separation into droplets with tunable viscosity and dynamics. Proc. Natl. Acad. Sci. USA 112, 7189–7194. https://doi. org/10.1073/pnas.1504822112.
- Heidenreich, M., Georgeson, J.M., Locatelli, E., Rovigatti, L., Nandi, S.K., Steinberg, A., Nadav, Y., Shimoni, E., Safran, S.A., Doye, J.P.K., et al. (2020). Designer protein assemblies with tunable phase diagrams in living cells. Nat. Chem. Biol. 16, 939–945. https://doi.org/10.1038/s41589-020-0576-z.
- Li, J., Kim, S.G., and Blenis, J. (2014). Rapamycin: One Drug, Many Effects. Cell Metab. 19, 373–379. https://doi.org/10.1016/j.cmet.2014. 01.001
- Miyamoto, T., DeRose, R., Suarez, A., Ueno, T., Chen, M., Sun, T.P., Wolfgang, M.J., Mukherjee, C., Meyers, D.J., and Inoue, T. (2012). Rapid and orthogonal logic gating with a gibberellin-induced dimerization system.
 Nat. Chem. Biol. 8, 465–470. https://doi.org/10.1038/nchembio.922.
- Liang, F.-S., Ho, W.Q., and Crabtree, G.R. (2011). Engineering the ABA Plant Stress Pathway for Regulation of Induced Proximity. Sci. Signal. 4, rs2. https://doi.org/10.1126/scisignal.2001449.
- An, L., Said, M., Tran, L., Majumder, S., Goreshnik, I., Lee, G.R., Juergens, D., Dauparas, J., Anishchenko, I., Coventry, B., et al. (2024). Binding and sensing diverse small molecules using shape-complementary pseudocycles. Science 385, 276–282. https://doi.org/10.1126/science.adn3780.
- Nandi, S.K., Österle, D., Heidenreich, M., Levy, E.D., and Safran, S.A. (2022). Affinity and Valence Impact the Extent and Symmetry of Phase Separation of Multivalent Proteins. Phys. Rev. Lett. 129, 128102. https://doi.org/10.1103/PhysRevLett.129.128102.
- Gao, Y., Li, X., Li, P., and Lin, Y. (2022). A brief guideline for studies of phase-separated biomolecular condensates. Nat. Chem. Biol. 18, 1307– 1318. https://doi.org/10.1038/s41589-022-01204-2.
- Villegas, J.A., Heidenreich, M., and Levy, E.D. (2022). Molecular and environmental determinants of biomolecular condensate formation. Nat. Chem. Biol. 18, 1319–1329. https://doi.org/10.1038/s41589-022-01175-4.
- Garcia-Jove Navarro, M., Kashida, S., Chouaib, R., Souquere, S., Pierron, G., Weil, D., and Gueroui, Z. (2019). RNA is a critical element for the sizing and the composition of phase-separated RNA-protein condensates. Nat. Commun. 10, 3230. https://doi.org/10.1038/s41467-019-11241-6.
- Ruskowitz, E.R., Munoz-Robles, B.G., Strange, A.C., Butcher, C.H., Kurniawan, S., Filteau, J.R., and DeForest, C.A. (2023). Spatiotemporal functional assembly of split protein pairs through a light-activated SpyLigation. Nat. Chem. 15, 694–704. https://doi.org/10.1038/s41557-023-01152-x.
- Munoz-Robles, B.G., and DeForest, C.A. (2024). Irreversible light-activated SpyLigation mediates split-protein assembly in 4D. Nat. Protoc. 19, 1015–1052. https://doi.org/10.1038/s41596-023-00938-0.
- 57. Kang, S., Davidsen, K., Gomez-Castillo, L., Jiang, H., Fu, X., Li, Z., Liang, Y., Jahn, M., Moussa, M., DiMaio, F., et al. (2019). COMBINES-CID: An efficient method for de novo engineering of highly specific chemically induced protein dimerization systems. J. Am. Chem. Soc. 141, 10948–10952. https://doi.org/10.1021/jacs.9b03522.
- Jumper, J., Evans, R., Pritzel, A., Green, T., Figurnov, M., Ronneberger, O., Tunyasuvunakool, K., Bates, R., Žídek, A., Potapenko, A., et al. (2021). Highly accurate protein structure prediction with AlphaFold. Nature 596, 583–589. https://doi.org/10.1038/s41586-021-03819-2.
- Bennett, N.R., Coventry, B., Goreshnik, I., Huang, B., Allen, A., Vafeados, D., Peng, Y.P., Dauparas, J., Baek, M., Stewart, L., et al. (2023). Improving de novo protein binder design with deep learning. Nat. Commun. 14, 2625. https://doi.org/10.1038/s41467-023-38328-5.